

See discussions, stats, and author profiles for this publication at: <https://www.researchgate.net/publication/262787732>

A DFT Study on the Mechanisms and Diastereoselectivities of Lewis Acid-Promoted Ketene-Alkene [2+2] Cycloadditions: What is the Role of Lewis Acid in the Ketene and C=X (X=O, CH₂,...)

ARTICLE *in* THE JOURNAL OF PHYSICAL CHEMISTRY A · MAY 2014

Impact Factor: 2.69 · DOI: 10.1021/jp500358m · Source: PubMed

CITATIONS

11

READS

30

5 AUTHORS, INCLUDING:



Donghui Wei

Zhengzhou University

65 PUBLICATIONS 506 CITATIONS

[SEE PROFILE](#)

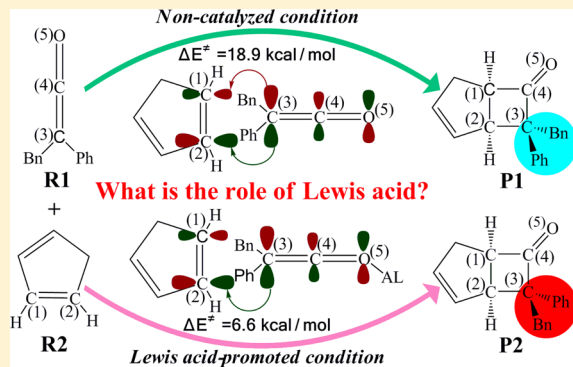
DFT Study on the Mechanisms and Diastereoselectivities of Lewis Acid-Promoted Ketene–Alkene [2 + 2] Cycloadditions: What is the Role of Lewis Acid in the Ketene and C = X (X = O, CH₂, and NH) [2 + 2] Cycloaddition Reactions?

Yang Wang, Donghui Wei,* Zhenyu Li, Yanyan Zhu, and Mingsheng Tang*

The College of Chemistry and Molecular Engineering, Center of Computational Chemistry, Zhengzhou University, Zhengzhou, Henan Province 450001, P.R. China

Supporting Information

ABSTRACT: The detailed mechanisms and diastereoselectivities of Lewis acid-promoted ketene–alkene [2 + 2] cycloaddition reactions have been studied by density functional theory (DFT). Four possible reaction channels, including two noncatalyzed diastereomeric reaction channels (channels A and B) and two Lewis acid (LA) ethylaluminum dichloride (EtAlCl_2) catalyzed diastereomeric reaction channels (channels C and D), have been investigated in this work. The calculated results indicate that channel A (associated with product R-configurational cyclopropanone) is more energy favorable than channel B (associated with the other product S-configurational cyclopropanone) under noncatalyzed condition, but channel D leading to S-configurational cyclopropanone is more energy-favorable than channel C, leading to R-configurational cyclopropanone under a LA-promoted condition, which is consistent with the experimental results. And Lewis acid can make the energy barrier of ketene–alkene [2 + 2] cycloaddition much lower. In order to explore the role of LA in ketene and C = X (X = O, CH₂, and NH) [2 + 2] cycloadditions, we have tracked and compared the interaction modes of frontier molecular orbitals (FMOs) along the intrinsic reaction coordinate (IRC) under the two different conditions. Besides by reducing the energy gap between the FMOs of the reactants, our computational results demonstrate that Lewis acid lowers the energy barrier of the ketene and C = X [2 + 2] cycloadditions by changing the overlap modes of the FMOs, which is remarkably different from the traditional FMO theory. Furthermore, analysis of global reactivity indexes has also been performed to explain the role of LA catalyst in the ketene–alkene [2 + 2] cycloaddition reaction.

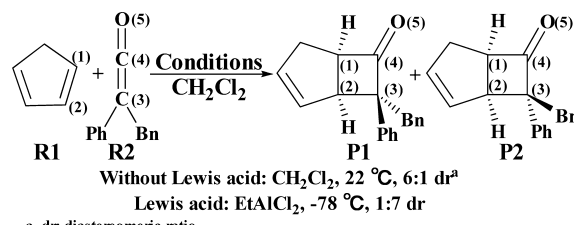


1. INTRODUCTION

A unique propensity in ketene chemistry is to give facile [2 + 2] cycloaddition reactions with compounds such as alkenes, ketones, imines, and so on.^{1–10} It was first reported by Staudinger in 1905,¹ and then many modifications and improvements introduced over the last hundred years had extended the versatility of ketene [2 + 2] cycloadditions.^{3,5,11,12} However, these noncatalyzed ketene [2 + 2] cycloaddition reactions between relatively unreactive reaction partners typically require forcing conditions. For example, Snider and co-workers explored a scope of intramolecular α, β -unsaturated ketene–alkene [2 + 2] cycloadditions with a yield of 75% in toluene at high temperature.¹³ Interestingly, many studies found that ketene and C = X (X = O and CH₂) [2 + 2] cycloaddition reactions can proceed easily with the presence of Lewis acid (LA),^{14–16} and it has been recently reported that Lewis base catalyst¹⁷ (such as NHC^{18–22}) can improve the stereoselectivity of the ketene [2 + 2] cycloaddition significantly. Notably, an outstanding example of ketene–alkene [2 + 2] cycloaddition reactions promoted by Lewis acid

(Scheme 1) is first reported by Rasik and co-workers.¹⁶ This method is notable for not only the substantial rate acceleration, the high yields, and good diastereoselectivities obtained for the formation of the cyclobutanone products but also the inverse

Scheme 1. Ketene–Alkene [2 + 2] Cycloadditions under Two Different Conditions



Received: January 12, 2014

Revised: May 27, 2014

Published: May 29, 2014

selectivity relative to traditional thermal cycloadditions observed for many ketene–alkene [2 + 2] cycloadditions. To the best of our knowledge, the mechanisms and diastereoselectivities of Lewis acid-promoted ketene–alkene [2 + 2] cycloadditions have not been investigated in theory, and why Lewis acid can promote the reaction and inverse the diastereoselectivity of the ketene–alkene [2 + 2] cycloadditions has remained unexplored until now.

Due to the special reactivity and wide applications on synthetic chemistry of the ketene [2 + 2] cycloadditions, they have also attracted more and more attention of theoretical chemists. To date, there have been many theoretical studies on the reaction mechanisms of ketene and C = X (X = O, CH₂, and NH) [2 + 2] cycloadditions under noncatalyzed conditions.^{23–40} For example, Rajzmann and co-workers studied two possible reaction paths leading from formaldehyde and ketene to 2-oxetanone under the noncatalyzed condition.²³ Truong investigated the effects of aqueous solvent on structures and mechanism of the [2 + 2] cycloaddition between ketene and imine by using correlated MP2 and MP4 levels of ab initio molecular orbital theory in conjunction with the dielectric continuum generalized conductor-like screening model (GCOSMO) for solvation. It was found that the reactions in the gas phase and in aqueous solutions had very different topology on the free-energy surfaces but had similar characteristic motion along the reaction coordinate.²⁴ Moreover, Xu and co-workers explored the annuloselectivity in the Staudinger reaction of ketenes with imines in three mechanistic possibilities of the [2 + 2] cycloaddition at the M06-2X(CPCM)//B3LYP(CPCM) levels of theory.²⁵ Cossio and coauthors studied the possible reaction paths corresponding to the noncatalyzed reaction between chloroketene (as a model activated ketene) and acetaldehyde (as a model alkyl carbonyl compound) using ab initio methodologies (MP2/6-31G*//HF/6-31G*).⁴¹ Houk et al. studied the reactions of ketene with ethylene (and of ketene with propene) using ab initio molecular orbital calculations, with the STO-3G, 3-21G, and 6-31G* basis set and correlation energy corrections at the MP2 level.²⁶ Recently, Kamiya and co-workers investigated the reaction pathway and diastereoselectivity diastereorecontrol mechanism of 2,4-pentanediol tether ketene-olefin [2 + 2] cycloadditions using ab initio molecular dynamics (AIMD) simulations.²⁷

In addition, there are several theoretical studies on the Lewis acid-catalyzed ketene and C=O [2 + 2] cycloadditions.^{41–43} Cossio and co-workers reported ab initio calculations (MP2/6-31G*//HF/6-31G*) on catalyst (BH₃), substituents, and solvent (CH₂Cl₂) effects for the cycloaddition reactions between ketene (or chloroketene) and formaldehyde (or acetaldehyde).^{41,42} Rajzmann and coauthors studied the formation of β -lactone through Lewis acid (BH₃ and BF₃) promoted ketene–ketone [2 + 2] cycloaddition using semi-empirical (AM1/RHF and AM1/CI) and ab initio (HF/6-31G* and MP2/6-31G*) calculations.⁴³ However, all these studies did not give a deep investigation on the frontier molecular orbital interaction under Lewis acid-catalyzed conditions, which should also be very important for the ketene [2 + 2] cycloaddition reactions.

Noteworthy, Yamabe et al. had provided the precise frontier molecular orbital (FMO) images for the ketene and C = X (X = O, CH₂, and NH) [2 + 2] cycloadditions under noncatalyzed condition by tracking the intrinsic reaction coordinate (IRC), and confirmed the FMOs participated in the ketene [2 + 2]

cycloaddition reactions,^{44,45} but they did not consider the influence of Lewis acid on the FMO interactions either. Moreover, our previous work first studied the mechanisms of Lewis acid BF₃-catalyzed ketene–ketone [2 + 2 + 2] cycloaddition reaction at the B3LYP/6-31G(d, p) level.⁴⁶ And our calculation results showed that the energy barrier of the rate-determining step (i.e., the [2 + 2] cycloaddition) has become much lower under Lewis acid-catalyzed condition, which is mainly due to the change of the overlap mode rather than the change of the orbital symmetries or energy gaps between the FMOs. Although we had explained the role of Lewis acid catalyst in the ketene and C=O [2 + 2] cycloaddition,⁴⁶ there are still some questions which need to be solved for the ketene and C = X (X = O, CH₂, and NH) [2 + 2] cycloadditions: (1) Does the Lewis acid catalyst have similar roles in the ketene and C = X (X = CH₂ and NH) [2 + 2] cycloadditions? (2) Is it general that the overlap modes between the FMOs of this kind of cycloadditions can be changed by the Lewis acid catalyst? (3) Under noncatalyzed and Lewis acid-catalyzed conditions, what is the difference of the overlap modes between the FMOs in ketene and C = X (X = CH₂ and NH) [2 + 2] cycloadditions? (4) For the traditional FMO theory, is it always right to just consider the symmetry and energy gaps of the FMOs of reactants? (5) In addition to the symmetry and energy gaps of the FMOs of reactants, is the overlap mode of FMOs also important for the cycloaddition reactions? (6) If there are several overlap modes of FMOs in the cycloadditions, which one should be the best? All above questions promote us to not only investigate the reaction mechanisms and diastereoselectivities of the ketene–alkene [2 + 2] cycloadditions but also explore the role of Lewis acid catalyst in the ketene and C = X (X = O, CH₂, and NH) [2 + 2] cycloadditions.

In the present study, the diastereomeric [2 + 2] cycloaddition reactions between cyclopentadiene (**R1**, Scheme 1) and benzyl(phenyl)ketene (**R2**, Scheme 1), under both the noncatalyzed and Lewis acid (EtAlCl₂)-catalyzed conditions, have been chosen as the objects of investigation. The reaction mechanisms and diastereoselectivities have been studied using density functional theory (DFT), which has been widely used in the study of organic,^{47–53} biological,^{54–56} and other reactions.^{57–61}

2. COMPUTATIONAL DETAILS

All DFT calculations were performed using Gaussian 09.⁶² The structures of the reactants, transition states, intermediates, and products in all reaction channels were optimized at the B3LYP^{63–65}/6-31G(d, p) level in CH₂Cl₂ solvent, using the integral equation formalism polarizable continuum model (IEF-PCM).^{66,67}

The corresponding vibrational frequencies were calculated at the same level to take account of the zero-point vibrational energy (ZPVE) and to identify the transition states which have one and only one imaginary frequency. And we also confirmed that all the reactants, intermediates, and products have no imaginary frequencies. The same level of intrinsic reaction coordinate (IRC)^{68,69} calculations were performed to ensure that the transition states lead to the expected reactants and products.

All the key stationary points involved in the paper were further refined at the 6-311++G(2d, 2p) single-point level in the solvent CH₂Cl₂ simulated by IEF-PCM, based on the geometries and zero-point vibration corrections calculated at

Scheme 2. Possible Mechanisms of Ketene–Alkene [2 + 2] Cycloadditions

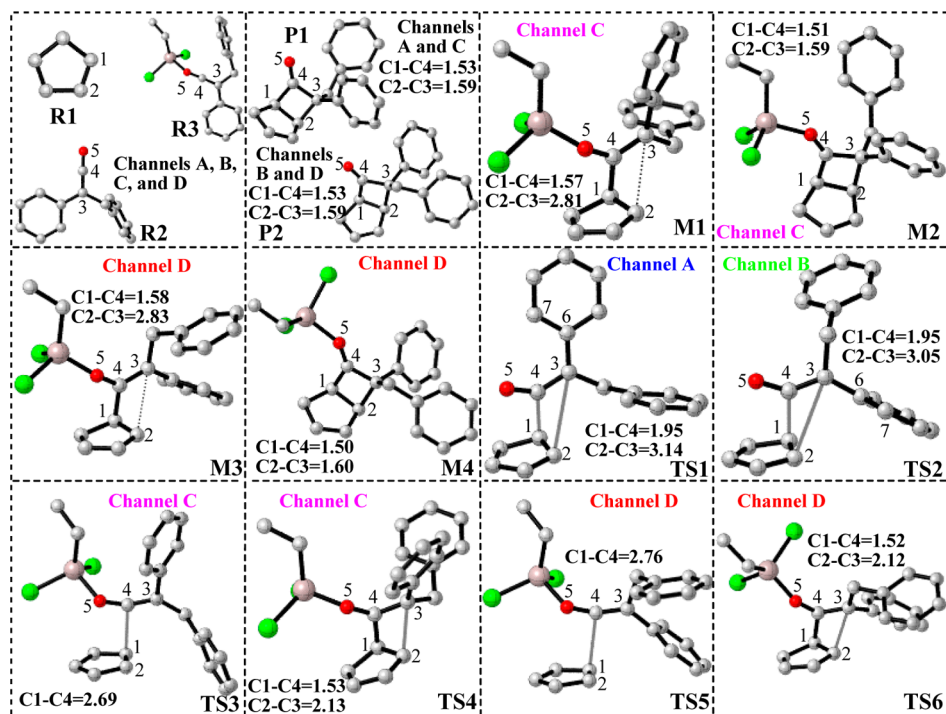
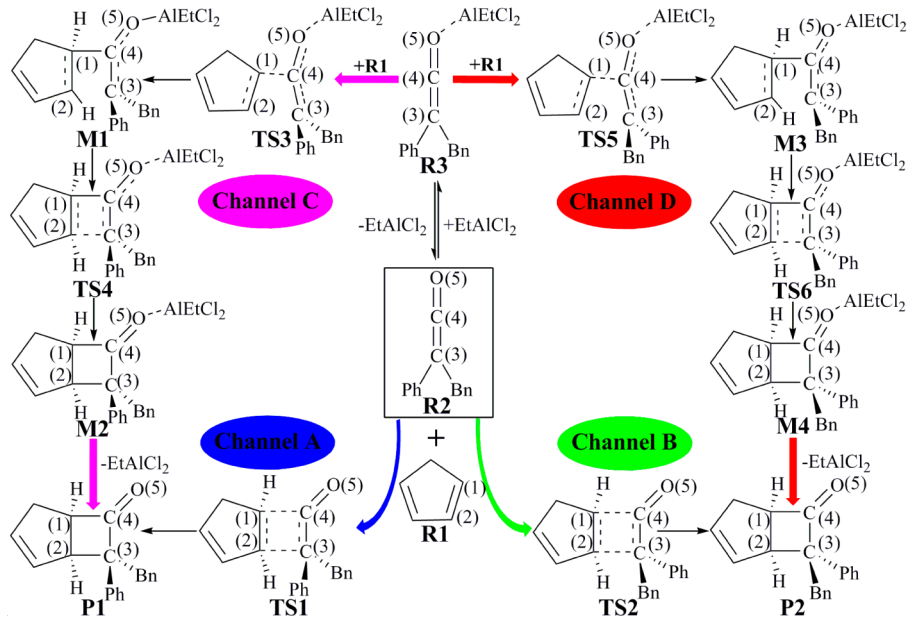


Figure 1. Structures and geometrical parameters of all the reactants, intermediates, transition states, and products optimized at the B3LYP/6-31G(d, p) level in CH_2Cl_2 solvent (length in angstroms). All the hydrogen atoms are omitted. Gray, red, green, and pink represent the carbon, oxygen, chorine, and aluminum, respectively.

the B3LYP level, which are generally known to be accurate.^{46,70–73}

All energy discussed in this paper, denoted $\Delta E_{\ddagger}^{\pm}$, are based on the electronic energy corrected for the zero-point vibration energies (ZPVEs) and calculated at the same level of theory.

3. RESULTS AND DISCUSSION

3.1. Reaction Mechanisms. On the basis of the experimental results, we have suggested and studied four possible channels (channels A, B, C, and D, Scheme 2), which

lead to two different products: P1 (syn-to-Bn) and P2 (syn-to-Ph). Figure 1 presents the structures and geometrical parameters of all the reactants, transition states, intermediates, and products optimized at the B3LYP/6-31G(d, p) level in CH_2Cl_2 solvent. We set the energies ($E + \text{ZPVE}$) of R1 + R2 and R1 + R3 as 0.0 kcal/mol as reference for noncatalyzed and Lewis acid-promoted channels in the potential energy profiles (Figure 2), respectively.

3.1.1. Noncatalyzed Ketene–Alkene [2 + 2] Cycloaddition Process. As shown in Scheme 2, there are two possible reaction channels (channels A and B) for the [2 + 2] cycloaddition

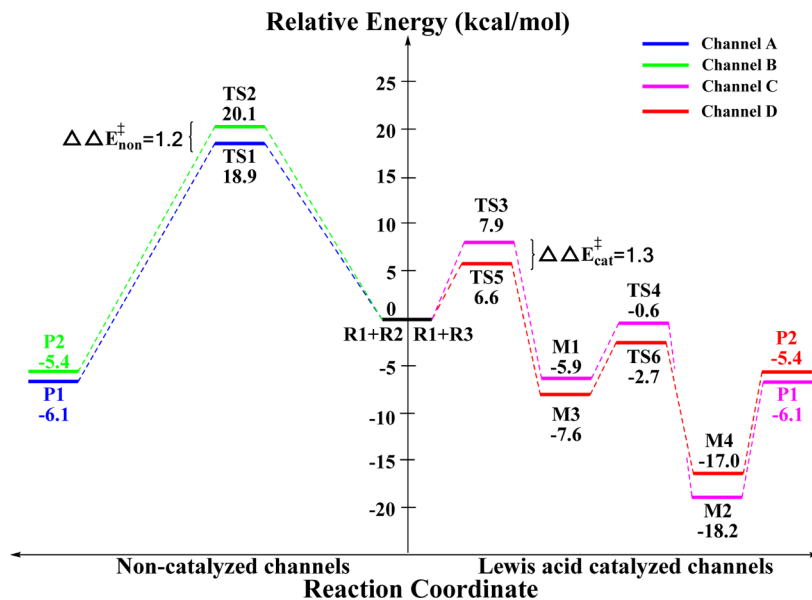


Figure 2. Energy profiles of four reaction channels.

process under noncatalyzed condition. The reactant R1 reacts with R2 to form cyclobutanone products P1 and P2 (Scheme 2) via transition states TS1 and TS2, respectively. In P1 and P2, the new single bonds C1–C4 and C2–C3 are formed, and the double bonds C1=C2 and C3=C4 become single bonds. With our calculated results, the noncatalyzed ketene–alkene [2 + 2] cycloaddition process is a concerted but nonsynchronous reaction.

It can be seen from Figure 1, the distances of C1–C4 and C2–C3 are 1.95 and 3.14 Å in transition state TS1 and change to 1.53 and 1.59 Å in product P1, respectively. The distances of C1–C4 and C2–C3 are 1.95 and 3.05 Å, respectively, in transition state TS2, then change to 1.53 and 1.59 Å in product P2, respectively. The energy barriers of channels A and B are 18.9 and 20.1 kcal/mol (Figure 2) respectively, indicating that channel A is more energy-favorable than channel B for the noncatalyzed [2 + 2] cycloaddition reaction.

3.1.2. Lewis Acid-Promoted ketene–Alkene [2 + 2] Cycloaddition Process. As can be seen from Scheme 2, initially, the reactant R2 combines with the catalyst EtAlCl₂ to form R3 in channels C and D. The calculated results demonstrate that the [2 + 2] cycloaddition is concerted process under noncatalyzed condition, but it changes to a stepwise manner under Lewis acid-promoted condition and there are two steps including the one center addition and ring closure steps. The detailed reaction processes are illustrated as follows.

There are two steps involved in Lewis acid-promoted reaction process, including the nucleophilic attack on C4 atom of R3 by C1 atom of R1 (the formation of C1–C4 bond) and the formation of the four-membered ring (C1–C2–C3–C4). In the first step of channel C, R1 reacts with R3 to form intermediate M1 (syn-to-Bn). In this step, the distance of C1–C4 changes from 2.69 Å in transition state TS3 to 1.57 Å in intermediate M1. The next step is the ring-forming process, which ultimately forms the C2–C3 bond. The distance of C2–C3 changes from 2.81 Å in M1 to 1.59 Å in M2 via TS4 (the distance of C2–C3 in TS4 is 2.13 Å). Similarly, the first step of channel D is also the formation of bond C1–C4, the distance of C1–C4 is shortened from 2.76 Å in transition state TS5 to

1.58 Å in intermediate M3 (syn-to-Ph). And the second step of channel D is to form four-membered ring intermediate M4, the distance of C2–C3 changes from 2.83 Å in M3 to 1.60 Å in M4 via TS6 (the distance of C2–C3 is 2.12 Å in TS6). Notably, the diastereomers P1 and P2 can be generated by the disassociation of Lewis acid EtAlCl₂ from the four-membered ring (C1–C2–C3–C4) intermediates (M2 and M4). We have tried many times but failed to locate the transition states for the dissociations of Lewis acid and products, and we cannot calculate the energy barriers of the dissociations. In addition, we have considered two possible pathways for the decomposition of catalyst dimer and tried many times to find the transition states depicted in Figure 3, but we did not locate the structures

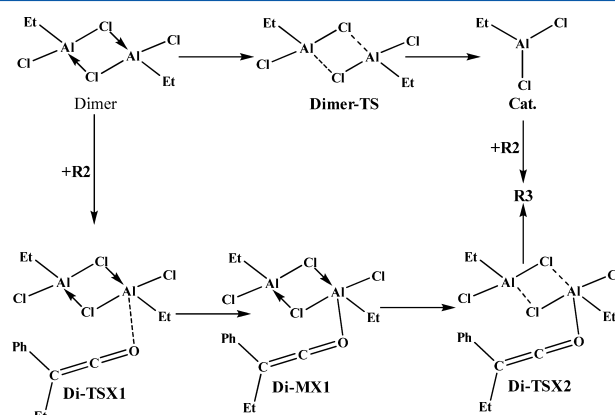


Figure 3. Possible pathways for the decomposition of catalyst dimer.

of those transition states. As presented in Figure 2, the dissociation process should be an endothermic process and not occur easily; this is in agreement with the experiment, in which the dissociation needs to warm from −78 °C to room temperature, and excess Lewis acid (2.5 equiv) is required because of product inhibition.

As shown in Figure 2, the energy barriers of the two steps in channel C are 7.9 and 5.3 kcal/mol, while those in channel D are 6.6 and 4.9 kcal/mol, respectively. So it is easy to see that

Scheme 3. Other Possible Mechanism Including Hetero-Diels-Alder [4 + 2] Cycloaddition and [3,3]-Claisen Rearrangement

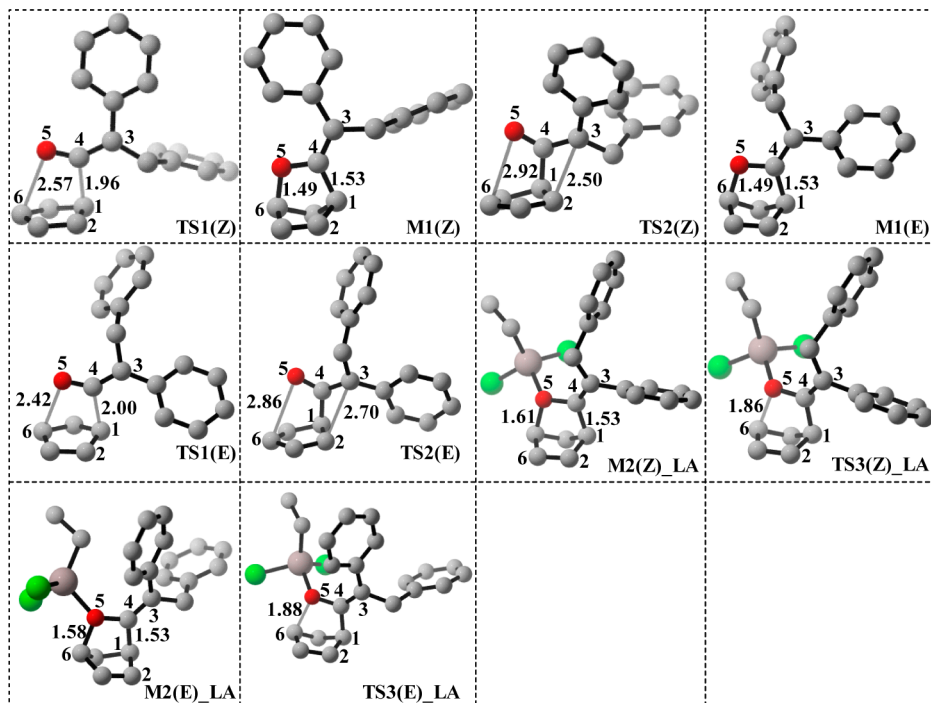
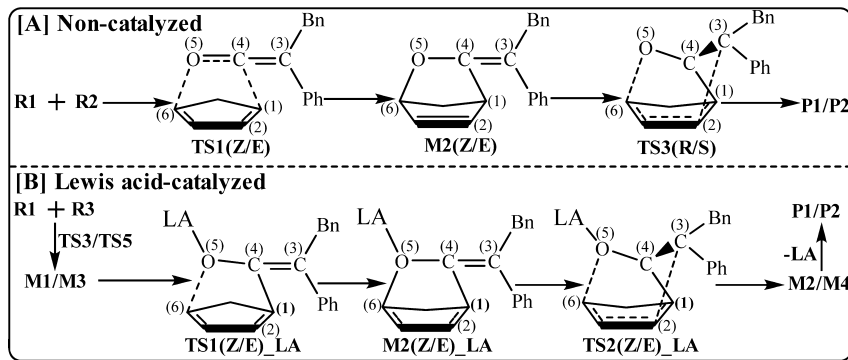


Figure 4. Structures and geometrical parameters of the intermediates and transition states optimized at the B3LYP/6-31G(d, p) level in CH_2Cl_2 solvent (length in angstroms). All the hydrogen atoms are omitted. Gray, red, green, and pink represent the carbon, oxygen, chorine, and aluminum, respectively.

the first step has the higher energy barrier in both channels C and D, that is to say, the formation of the C1–C4 bond is the rate-determining step, and channel D (associated with the energy barrier of 6.6 kcal/mol) is more energy favorable than channel C (associated with the energy barrier of 7.9 kcal/mol) under Lewis acid-catalyzed condition.

In summary, the energy barriers of the noncatalyzed channels (channels A and B) are 18.9 and 20.1 kcal/mol, respectively, and those of entire Lewis acid-promoted channels (channels C and D) are much lower (7.9 and 6.6 kcal/mol). Obviously, channel A is energy favorable and **P1** should be the main product under the noncatalyzed condition, but under the Lewis acid-promoted condition, channel D is energy favorable and **P2** is the main product. The computational results are well consistent with the experimental results, and we have explored the reason for the inverse diastereoselectivity under the two different conditions in the following part.

3.1.3. Other Possible Mechanism. Additionally, we have suggested and investigated another possible mechanism, which

contains two processes (i.e., hetero-Diels–Alder [4 + 2] cycloaddition and [3,3]-Claisen rearrangement) (Scheme 3).^{35,74} It should be noted that the hetero-Diels–Alder [4 + 2] cycloaddition process becomes the stepwise manner, and shares the same first step depicted in channels C and D. Figures 4 and 5 show the optimized structures of the stationary points and the corresponding energy profiles, respectively. A comparison of Figures 2 and 5 shows the computational energy barriers of the four reaction channels in Figure 5 to be obviously higher than those in Figure 2 under both the noncatalyzed and Lewis acid-catalyzed conditions. Thus, we conclude the most favorable channels should be the direct [2 + 2] cycloaddition reaction channels (channels A, B, C, and D). And we think it should be useless to consider the [3,3]-Claisen rearrangement process under the Lewis acid-catalyzed condition.

3.1.4. Origin of Diastereoselectivities in the Ketene–Alkene [2 + 2] Cycloadditions. On the basis of conclusions obtained in the previous subsection, it can be found that the

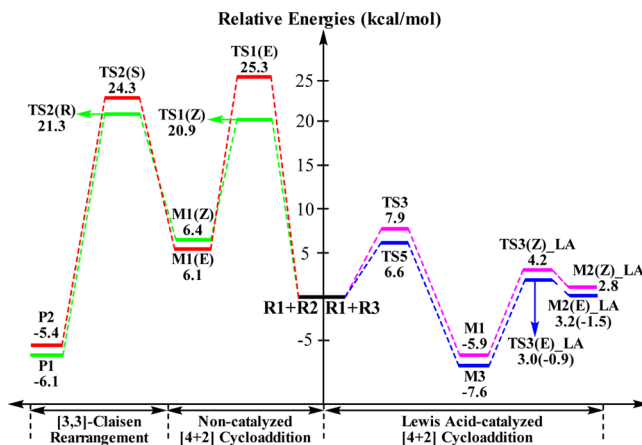
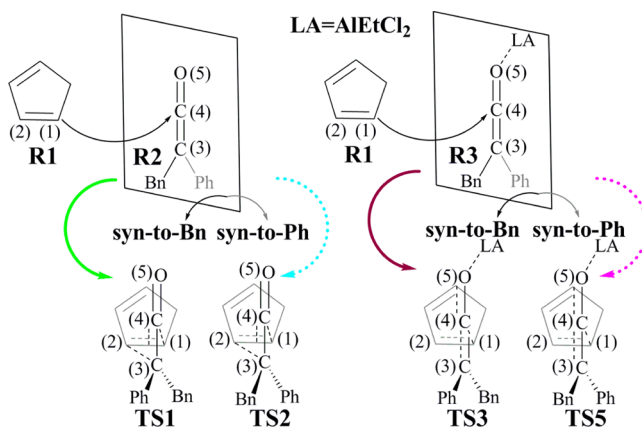


Figure 5. Energy profiles of the other possible mechanism.

rate-determining steps are also the diastereoselectivity-determining steps in the ketene–alkene [2 + 2] cycloadditions. So the transition states TS1, TS2, TS3, and TS5 are the key for the diastereoselectivities of the reactions. As depicted in Figure 2, $\Delta\Delta E_{\text{non}}^{\ddagger}$ represents the difference between the energy barriers of channels A and B ($\Delta\Delta E_{\text{non}}^{\ddagger} = \Delta E_{\text{TS2}}^{\ddagger} - \Delta E_{\text{TS1}}^{\ddagger}$) and $\Delta\Delta E_{\text{cat}}^{\ddagger}$ represents the difference between the energy barriers of channels C and D ($\Delta\Delta E_{\text{cat}}^{\ddagger} = \Delta E_{\text{TS3}}^{\ddagger} - \Delta E_{\text{TS5}}^{\ddagger}$), which are calculated to be 1.2 and 1.3 kcal/mol, respectively. In accordance with the experimental outcomes,¹⁴ the diastereomeric ratios (dr) are 6:1 (P1:P2) under noncatalyzed condition and 1:7 (P1:P2) under Lewis acid-promoted condition, respectively, which indicates that the difference between the energy barriers of channels C and D should be a little bigger than that of channels A and B; this demonstrates that our calculated results are in agreement with the experiment.

As depicted in Scheme 4, the prearranged conformations for the encounter of R2 (or R3) and R1 are antarafacial and

Scheme 4. Stereochemistry in the Ketene–Alkene [2 + 2] Cycloaddition Reactions



orthogonal, and the steric configuration (syn-to-Bn or syn-to-Ph) of the transition states leads to the different diastereoselectivities of the products. To obtain further insight into the diastereoselectivities of the reactions, we examined and compared the exact geometries of the transition states in the rate-determining steps of the four channels. In the structures of TS1 and TS2 (Figure 1), the dihedral angles of C4–C3–C6–C7 are -3.36° and -106.41° , respectively, which reveals that

the benzene group and C3=C4 double bond are nearly coplanar in TS1. As the result, TS1 should be more stable than TS2, which is due to the formation of conjugated system between the benzene group and C3=C4 double bond in TS1. In regard to Lewis acid-promoted condition, there is no formation of conjugated system in both TS3 and TS5. However, the distance of C1–C4 in transition state TS5 (2.76 Å, Figure 1) is longer than that in transition state TS3 (2.69 Å, Figure 1), and the benzyl group of R3 are closer to R2 in TS3 while the phenyl group of R3 are closer to R2 in TS5, which demonstrates that the steric effect between the two reactants (R2 and R3) might be weaker in TS5 than that in TS3. Thus, TS5 would be more stable than TS3.

3.1.5. Solvation Effect. Furthermore, we optimized the reaction species involved in the [2 + 2] cycloaddition reactions at B3LYP/6-31G(d, p) level in gas phase and further refined the single-point energies at the 6-311++G(2d, 2p) level. The calculated results indicate that the differences between the geometries optimized in solvent and those in vacuum are very tiny. And the energy barriers in both CH₂Cl₂ and gas phase have been summarized in Table 1. As shown in Table 1, the

Table 1. Relative Energies of the Species for the [2 + 2] Cycloadditions at the B3LYP/6-311++G(2d, 2p)//B3LYP/6-31G(d, p) Level in CH₂Cl₂ and Gas Phase^a

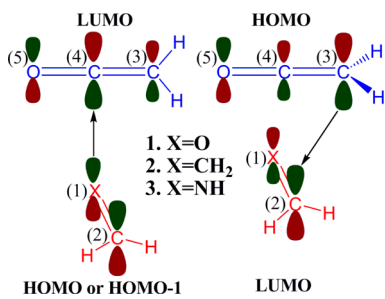
species	6-311++G(2d, 2p) in CH ₂ Cl ₂	6-311++G(2d, 2p) in gas phase
R1+R2	0.0	0.0
TS1	18.9	20.6
TS2	20.1	21.6
P1	-6.1	-5.6
P2	-5.4	-5.3
R1+R3	0.0	0.0
TS3	7.9	8.1
M1	-5.9	-1.4
TS4	-0.6	2.4
M2	-18.2	-17.7
TS5	6.6	6.3
M3	-7.6	-3.0
TS6	-2.7	0.4
M4	-17.0	-16.2

^aUnit: kilocalories per mole.

energy barriers of the channels A, B, C, and D in CH₂Cl₂ are 18.9, 20.1, 7.9, and 6.6 kcal/mol, respectively, whereas those in gas phase are 20.6, 21.6, 8.1, and 6.3 kcal/mol, separately, indicating that the solvation effect has little influence on the [2 + 2] cycloaddition reactions.

3.2. Frontier Molecular Orbital (FMO) Analysis. As discussed above, the energy barriers of Lewis acid-promoted [2 + 2] cycloaddition processes are much lower than those of the noncatalyzed [2 + 2] cycloaddition process. In order to explain this phenomenon and understand the role of Lewis acid EtAlCl₂, we compared the differences between the frontier molecular orbitals with and without the presence of LA catalyst. Noteworthy, as shown in Scheme 5, Yamabe et al. thought that the two one-center frontier molecular orbital interactions took place independently in the ketene and C = X (X = O, CH₂, and NH) [2 + 2] cycloadditions under noncatalyzed condition; the left interaction in Scheme 5 would lead to the formation of C1–C4 σ bond, and the right interaction in Scheme 5 would lead to the formation of C2–C3 σ bond; the two one-center

Scheme 5. Two One-Center Frontier Molecular Orbital (FMO) Interactions of Ketene and C = X (X = O, CH₂, and NH) [2 + 2] Cycloaddition



molecular orbital interactions are not concerned with orbital symmetries.⁴⁴

On the basis of the interactions depicted in Scheme 5, we think that the two one-center frontier molecular orbital interactions of the ketene–alkene [2 + 2] cycloaddition should be corresponding to the interaction between LUMO_{R2} and HOMO_{R1} (associated with the formation of C1–C4 bond) and that between LUMO_{R1} and HOMO_{R2} (associated with the formation of C2–C3 bond), respectively. And the calculated FMOs and the energy gaps between HOMOs and LUMOs of reactants under noncatalyzed and Lewis acid-promoted conditions are depicted in Figure 6. As shown in Figure 6,

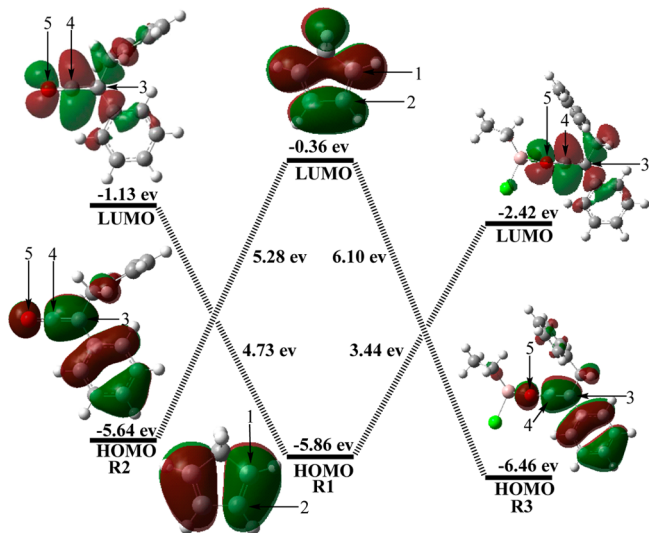


Figure 6. FMOs of R1, R2, and R3 calculated at the B3LYP/6-31G(d, p) level in the CH₂Cl₂ solvent (unit: eV).

there is almost no difference between the FMO pictures of reactants with and without the presence of LA. The energy gap between HOMO_{R1} and LUMO_{R3} becomes narrower than that between HOMO_{R1} and LUMO_{R2}, which demonstrates that the C1–C4 bond will form more smoothly when using EtAlCl₂ as the catalyst. However, the energy gap between LUMO_{R1} and HOMO_{R3} under Lewis acid-promoted conditions becomes wider than that between LUMO_{R1} and HOMO_{R2}, indicating that the LA catalyst cannot promote the interaction; this seems to be against with the experimental results. Moreover, the head-to-head overlap mode of the interaction between LUMO_{R1} and HOMO_{R2} (or HOMO_{R3}) seems to be “symmetry-forbidden” for the formation of the four-membered ring (C1–C2–C3–C4), since the orbital of C1=C2 bond in LUMO_{R1} is π^* ,

whereas the orbital of C3=C4 bond in HOMO_{R2} (or HOMO_{R3}) is π (Figure 5). If the FMO interactions are not concerned with orbital symmetries, why can the two σ bonds (C1–C4, C2–C3) not generate synchronously via the above transition states? Now all the questions are focused on the interaction between LUMO_{R1} and HOMO_{R2} (or HOMO_{R3}). For example, (1) how does the “symmetry-forbidden” interaction occur, and (2) how does the LA catalyst promote this interaction (associated with the formation of the C2–C3 σ bond)?

In order to solve these questions, we tracked and compared the interactions between LUMO_{R1} and HOMO_{R2} (and HOMO_{R3}) under the two different conditions. It should be noted that the interactions between LUMO_{R1} and HOMO_{R2} (and HOMO_{R3}) can be examined by tracking the changes of FMOs along the intrinsic reaction coordinate (IRC) of the transition states.^{44–46} Regardless of the diastereoselectivity, the IRC results of transition state TS2 were studied for the noncatalyzed condition, while those of transition states TS3 and TS4 were investigated for Lewis acid-promoted condition.

Figures 7 and 8 show the possible overlap modes of the FMOs. As can be seen from Figure S1 of the Supporting Information; initially the π^* orbital (R1) and the π orbital (R2) cannot overlap as a head-to-head mode (mode A in Figure 7A) but can overlap as a shoulder-to-head mode (mode B in Figure 7A). Subsequently, the shoulder-to-head overlap mode no longer exists, and there is only the one-center head-to-head overlap mode (mode E in Figure 8A) after the formation of the C1–C4 σ bond. Notably, the π orbital of HOMO_{R2} overlapping with the π^* orbital of LUMO_{R1} can only lead to the formation of the C2–C3 σ orbital, which is consistent with the study of Yamabe and coauthors.⁴⁴

In addition, we have also observed the interaction between LUMO_{R1} and HOMO_{R3} by tracking the orbital changes along the IRC of TS3 (Figure S2 of the Supporting Information) and TS4 (Figure S3 of the Supporting Information) under a LA-promoted condition. As presented in Figure S2 of the Supporting Information, the FMOs of two reactants are also “symmetry-forbidden” (mode C in Figure 7B), but they can overlap as a half shoulder-to-head mode (mode D in Figure 7B) with R1 getting close to R3. Although the energies of the HOMOs in the IRC points also become higher and higher accompanied by overlapping by the half shoulder-to-head mode (Figure S2 of the Supporting Information), these are much lower than those accompanied by overlapping by the shoulder-to-head mode (Figure S1 of the Supporting Information). After the formation of C1–C4 σ bond in intermediate M1, the half shoulder-to-head mode disappears and only a one-center head-to-head overlap mode (mode F in Figure 8B) exists in the IRC points of TS4 (Figure S3 of the Supporting Information).

As concerned as above, it is easy to find that the head-to-head “symmetry-forbidden” overlap mode (modes A and C in Figure 7) seems to become a one-center head-to-head “symmetry-matched” overlap mode (modes E and F in Figure 8) after the formation of the C1–C4 σ bond. As can be seen from Figures S1 and S2 of the Supporting Information, the FMO interactions in Scheme 5 will be changed in the presence of the catalyst, which should be responsible for the different mechanisms under the two different conditions. By comparing the two different orbital overlap modes (mode B + E under noncatalyzed condition and mode D + F under LA-promoted condition), and the energy barriers associated with them, we can conclude that the half shoulder-to-head overlap mode

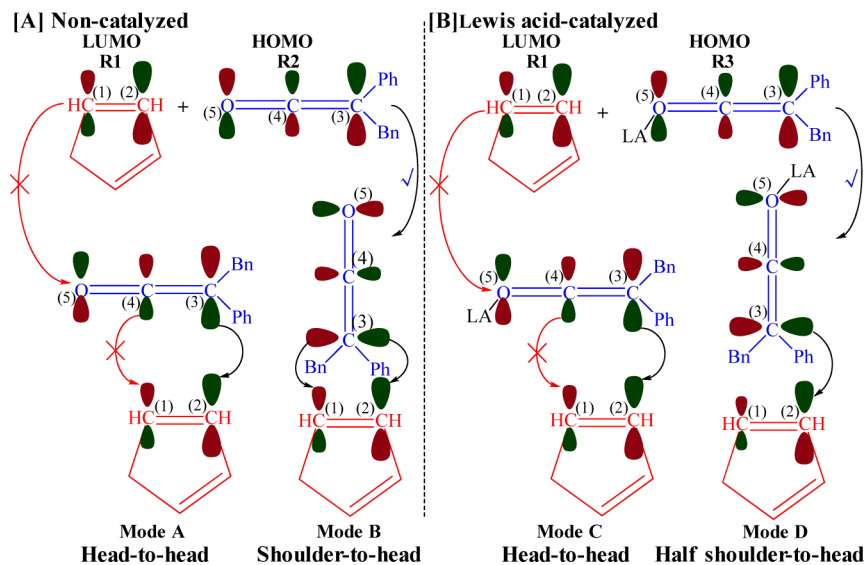


Figure 7. Different overlap modes between LUMO_{R1} and HOMO_{R2} (or HOMO_{R3}) before the formation of the C1–C4 bond.

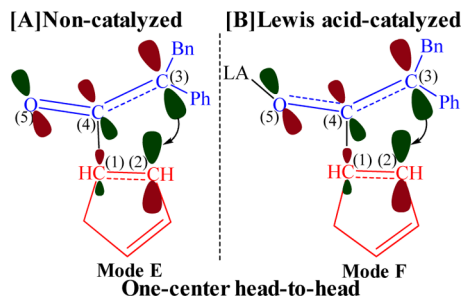


Figure 8. Same overlap modes between the FMOs after the formation of C1–C4 bond.

(Mode D in Figure 7B) should be more energy favorable than the shoulder-to-head overlap mode (mode B in Figure 7A), and the LA EtAlCl₂ can promote the formation of the C2–C3 σ bond by changing the overlap mode rather than effecting the

orbital symmetries and energy gaps between LUMO_{R1} and HOMO_{R2}.

Noteworthy, our previous work indicates that the overlap mode (shoulder-to-head mode and one-center head-to-head mode) under noncatalyzed condition changes to only a one-center head-to-head mode under LA BF₃-catalyzed condition for the formation of the C2–C3 σ bond, which also makes the energy barrier of ketene and C=O [2 + 2] cycloaddition much lower. Thus, it can be concluded that the head-to-head overlap mode should be the best way for the formation of the C2–C3 σ bond, and Lewis acid catalysts play the similar role in the ketene and C = X (X = O and CH₂) [2 + 2] cycloadditions.

3.3. Mechanism and Frontier Molecular Orbital Analysis of Ketene–Imine [2 + 2] Cycloadditions. As we all know, the ketene–imine [2 + 2] cycloaddition is also a member of the ketene [2 + 2] cycloaddition family, so we want to know if Lewis acid plays a similar role in the ketene–imine [2 + 2] cycloadditions. Herein, we have also studied the

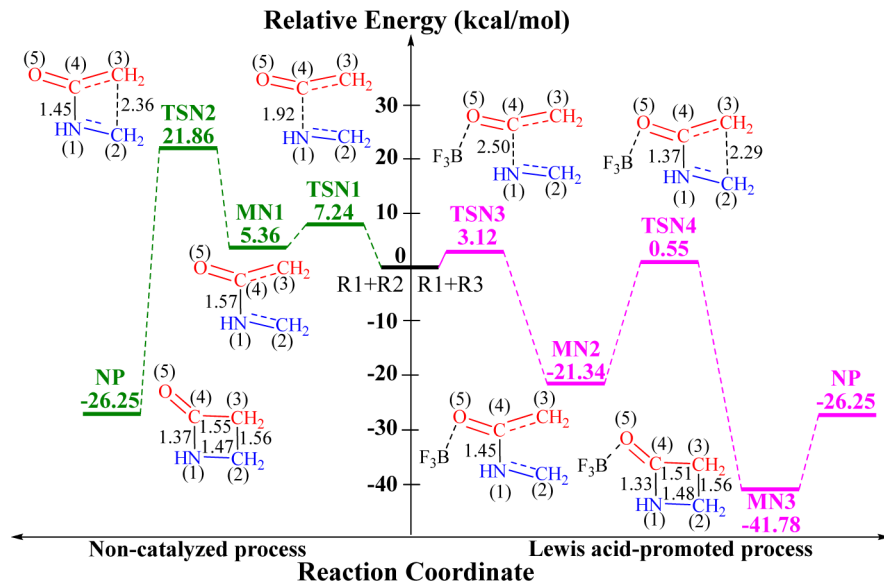


Figure 9. Key geometrical parameters and energy profiles of methanimine–ethenone [2 + 2] cycloaddition (length in angstroms).

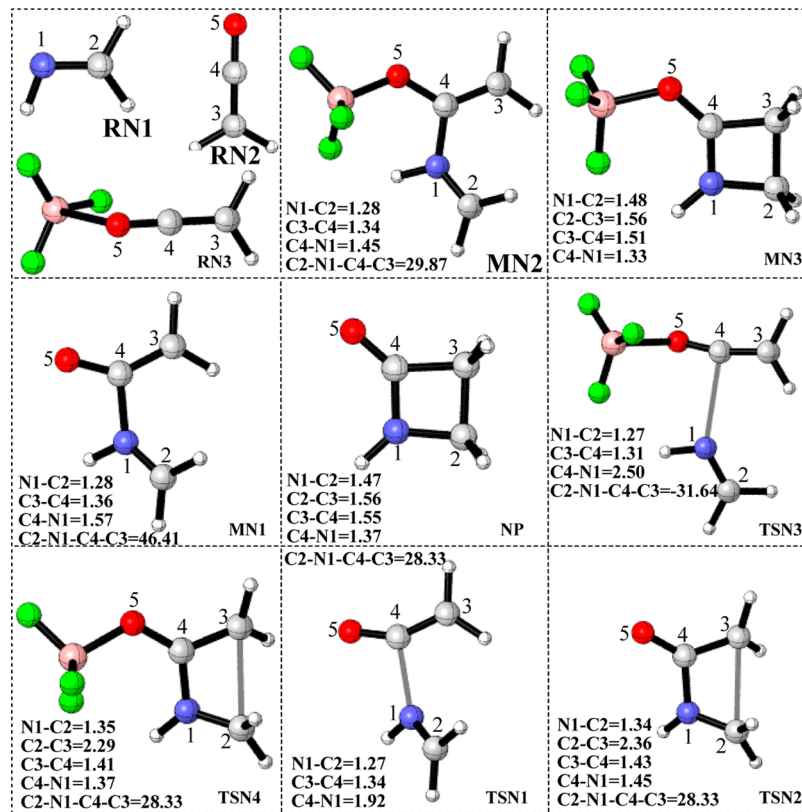


Figure 10. Structures and the geometrical parameters of all the reactants, intermediates, transition states, and product optimized at the B3LYP/6-31G(d, p) level in the CH_2Cl_2 solvent. Distance in angstroms and dihedral angle in degrees. Gray, white, red, blue, green, and pink represent the carbon, hydrogen, oxygen, nitrogen, fluorine, and boron, respectively.

mechanisms and FMO interactions of the ketene-imine [2 + 2] cycloaddition reaction under noncatalyzed and LA BF_3 -catalyzed conditions. For the reaction between ketene and $\text{C}=\text{N}$ bond, we just choose the simplest model, which has also been investigated by other theoretical scientists.⁷⁵ The methanimine and ethenone was chosen as the reactants. The key stationary points and the corresponding energy profiles of the methanimine–ethenone cycloadditions are shown in Figure 9, and the structures of all reactants, transition states, intermediates, and product optimized at the B3LYP/6-31G(d, p)//B3LYP/6-311++G(2d, 2p) level in CH_2Cl_2 solvent are depicted in Figure 10.

The calculated results indicate that both of the noncatalyzed and Lewis acid BF_3 -catalyzed cycloaddition processes are stepwise (i.e., the nucleophilic attack of RN1 to RN2 or RN3 and the ring-forming process), which is very different from the ketene–ketone/alkene [2 + 2] cycloadditions. As can be seen from Figure 9, the highest energy barrier of the BF_3 -catalyzed cycloaddition process is 21.89 kcal/mol, and that of the noncatalyzed cycloaddition process is 21.86 kcal/mol, which demonstrates that Lewis acid does not promote the ketene-imine [2 + 2] cycloaddition reaction at all; this is in good agreement with the experiment that the ketene-imine [2 + 2] cycloadditions can occur under mild conditions.^{25,75} We have tried many times but failed to locate the transition states for the dissociations of Lewis acid and products, and we cannot calculate the energy barriers of the dissociations. As shown in Figure 9, the dissociation process should also be an endothermic process and not easily happen.

As shown in Figures 5 and 11, the symmetry and energy gaps between the FMOs of reactants in ketene-alkene and ketene-

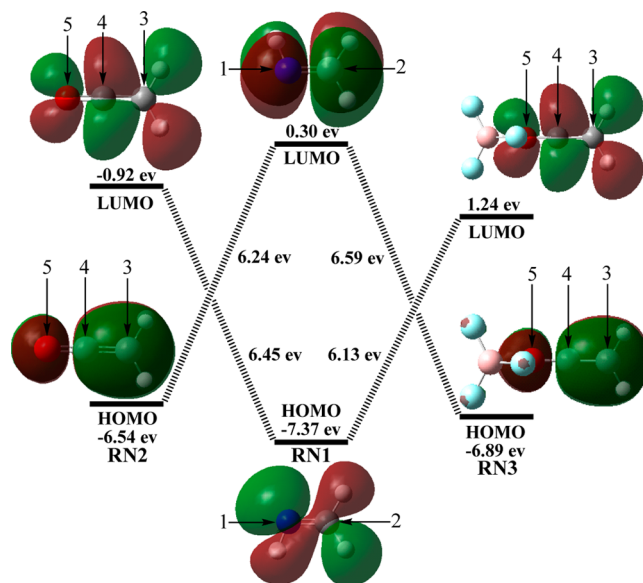


Figure 11. Calculated FMOs of RN1, RN2, and RN3 at the B3LYP/6-31G(d, p) level in a CH_2Cl_2 solvent (unit: eV).

imine [2 + 2] cycloadditions are very similar and have the same questions under the two conditions, so the LA should have the same role based on traditional FMO theory. However, our calculated results indicate that LA plays a very different role in the ketene-alkene and ketene-imine [2 + 2] cycloadditions; that is to say, there is another problem in understanding the role of LA in this kind of reaction in the traditional FMO

theory. Furthermore, if our conclusion that LA lowers the energy barrier mainly by changing the overlap mode of FMOs is right, then we can give another hypothesis (i.e., the LA would not lower the energy barrier if it does not change the overlap mode of FMOs), which has been confirmed as follows:

Similar with the FMOs in the above ketene–alkene [2 + 2] cycloaddition, the HOMOs of IRC points in **TSN1** and **TSN2** (IRC-1 depicted in Figure S4 of the Supporting Information) are corresponding to $\text{HOMO}_{\text{RN}2}$ (Figure 11). Several representative orbital structures of **TSN2**'s IRC points are depicted in Figure S4 of the Supporting Information, the orbital of the C2 atom overlaps with the orbital of the C3 atom mainly by a one-center head-to-head overlap mode (like mode E in Figure 8A) accompanied by the C2 atom getting close to the C3 atom. Figure S5 of the Supporting Information presents the $\text{HOMO}_{\text{TSN}3}$, $\text{HOMO}_{\text{MN}2}$, and several representative HOMOs of the IRC points in **TSN4**. Similarly, the $\text{HOMO}_{\text{TSN}3}$ and $\text{HOMO}_{\text{MN}2}$ are corresponding to $\text{HOMO}_{\text{RN}3}$. As depicted in Figure S5 of the Supporting Information, the N1–C4 bond has been generated in **MN2**, and the orbital of the C2 atom also overlaps with the orbital of the C3 atom mainly by a one-center head-to-head mode (like mode F in Figure 8B) with the C2 atom getting close to the C3 atom.

As concerned as above, the overlap mode of FMOs (i.e., the one-center head-to-head overlap mode) in ketene–imine [2 + 2] cycloaddition under noncatalyzed condition is almost the same with that under BF_3 -catalyzed conditions. So it is not surprising that the LA BF_3 do not lower the energy barrier of ketene–imine [2 + 2] cycloaddition, and this can explain that the LA catalyst seems to be unnecessary for the ketene–imine [2 + 2] cycloadditions.

3.4. Analysis of the Global Reactivity Indexes of the Reactants.

As shown in Table 2, the molecular global

Table 2. Energy of HOMO (E_H , a.u.), Energy of LUMO (E_L , a.u.), Electronic Chemical Potential (μ , in a.u.), Chemical Hardness (η , in a.u.), Global Electrophilicity (ω , in eV), and Global Nucleophilicity (N, in eV) of Some Reactants (SR)

SR	E_H (a.u.)	E_L (a.u.)	μ (a.u.)	η (a.u.)	ω (eV)	N (eV)
R1	−0.215	−0.013	−0.114	0.202	0.871	2.943
R2	−0.207	−0.042	−0.1245	0.166	1.279	3.164
R3	−0.238	−0.089	−0.163	0.149	2.449	2.339

electrophilicity character is measured by the electrophilicity index ω ,⁷⁶ which is calculated by the following expression, $\omega = (\mu^2/2\eta)$,^{76–79} in terms of the electronic chemical potential μ and the chemical hardness η . Both quantities may be approached in terms of the one-electron energies of the frontier molecular orbital HOMO and LUMO (E_H and E_L), as $\mu \approx (E_H + E_L)/2$ and $\eta \approx (E_L - E_H)$.

In accordance with the HOMO energies obtained within the Kohn–Sham scheme,^{80,81} Domingo and co-workers gave the nucleophilicity index N to handle a nucleophilicity scale.^{78,82–85} The nucleophilicity index is defined as $N = E_{\text{HOMO}(\text{SR})} - E_{\text{HOMO}(\text{TCE})}$. The nucleophilicity scale is referred to tetracyanoethylene (TCE) taken as a reference. Following these indices definitions, in this reaction, **R3** is classified as the electrophile ($\omega = 2.449\text{eV}$), **R1** is the nucleophile with the value of 2.943eV . The electrophilic value of **R3** is obviously larger than that of **R2**, indicating that Lewis acid EtAlCl_2 noticeably strengthens the electrophilicity of the reactant **R2** and thus decreases the energy barrier of the [2 + 2] cycloaddition.

4. CONCLUSIONS

The DFT calculations carried out in this work have afforded the detailed computational study on possible mechanisms and diastereoselectivities for the ketene–alkene [2 + 2] cycloaddition reactions. We have studied four possible reaction channels (channels A, B, C, and D) of the ketene–alkene [2 + 2] cycloaddition reaction with **P1** and **P2** as the products at the B3LYP/6-31G(d, p) level in CH_2Cl_2 solvent using the IEF-PCM model. The calculated results demonstrate that the reaction channel A is an energy favorable channel in the noncatalyzed process which generates the diastereomeric product **P1**, while the channel D is an energy favorable channel in the Lewis acid-promoted process which is associated with the diastereomeric product **P2**. And the concerted reaction process under noncatalyzed conditions has become a stepwise reaction process under the Lewis acid-promoted condition. Moreover, our calculated results confirm that the yields and diastereoselectivities have been improved, and diastereoselectivity has been inverted by the Lewis acid catalyst.

On the basis of the calculated FMO pictures, we found that problems exist with using the traditional FMO theory to explain the role of the LA catalyst in ketene and $\text{C} = \text{X}$ ($\text{X} = \text{O}, \text{CH}_2$, and NH) [2 + 2] cycloadditions. In order to explore the role of LA in these cycloaddition reactions, the method of tracking FMOs in the IRC points of the [2 + 2] transition states has been employed not only to confirm the FMOs of reactants involved in the cycloadditions but also to study the overlap modes of the FMOs. Our computational results demonstrate that Lewis acid can lower the energy barrier of the ketene and $\text{C} = \text{X}$ ($\text{X} = \text{O}$ and CH_2) [2 + 2] cycloaddition reactions, which is mainly due to the change in the overlap mode rather than the orbital symmetries and energy gaps between the FMOs of the reactants. And this hypothesis has also proved to be correct in the ketene and $\text{C}=\text{NH}$ [2 + 2] cycloaddition. Therefore, this work should be useful for chemists on the catalyst design of cycloaddition reactions in the near future. Further, the analysis of the global reactivity indexes of the ketene–alkene [2 + 2] cycloaddition reactions has been performed to explore the role of Lewis acid EtAlCl_2 , and the results indicate that the coordination of EtAlCl_2 to the ketene oxygen atom of **R2** noticeably strengthens the electrophilicity of the reactant, therefore, the energy barrier of the [2 + 2] cycloaddition decreases significantly. For both mechanisms and FMO discussions, we have considered and studied the role of the Lewis acid catalyst in the ketene and $\text{C} = \text{X}$ ($\text{X} = \text{O}, \text{CH}_2$, and NH) [2 + 2] cycloaddition reactions, which is remarkably different from Yamabe's work.

Over the past several decades, the FMO theory pioneered by Fukui has been recognized as a powerful tool to study and even predict the cycloaddition reactions, and the symmetry and energy gaps between the FMOs of reactants are the key to solve the chemical questions in Fukui's FMO theory (i.e., the traditional FMO theory). However, based on the calculated results in this work, we found that only the symmetry and energy gaps between the FMOs of reactants cannot exactly explain and predict the role of LA catalyst in the ketene and $\text{C} = \text{X}$ ($\text{X} = \text{O}, \text{CH}_2$, and NH) [2 + 2] cycloaddition reactions, and the different overlap modes of the FMOs should be the real key to explain the role of LA in the ketene [2 + 2] cycloaddition reactions. Therefore, this work should be helpful for not only understanding the role of LA in this kind of

reactions but also providing valuable clue for the development of the FMO theory.

■ ASSOCIATED CONTENT

S Supporting Information

Cartesian coordinates and the ZPVE of all the stationary points obtained at the B3LYP/6-31G(d, p) level in gas phase and the solvent CH₂Cl₂ using IEF-PCM model. And the Cartesian coordinates, energies, FMO images, and key distances of several representative IRC points of transition states TS2, TS3, TS4, TSN1, TSN2, TSN3, and TSN4 obtained at the same level. The complete citation of ref 62. The refined energies of all the above optimized structures calculated at the B3LYP/6-311+ +G(2d, 2p) level in the solvent CH₂Cl₂ using an IEF-PCM model. This material is available free of charge via the Internet at <http://pubs.acs.org>.

■ AUTHOR INFORMATION

Corresponding Authors

*E-mail: donghuiwei@zzu.edu.cn.

*E-mail: mstang@zzu.edu.cn. Tel: +86 037167781815.

Notes

The authors declare no competing financial interest.

■ ACKNOWLEDGMENTS

We acknowledge financial support from the National Natural Science Foundation of China (Grant 21303167) and the China Postdoctoral Science Foundation (Grant 2013MS30340).

■ REFERENCES

- (1) Staudinger, H. Ketene, Eine Neue Körperklasse. *Chem. Ber.* **1905**, *38*, 1735–1739.
- (2) Staudinger, H. Über Ketene. 4. Mitteilung: Reaktionen des Diphenylketens. *Chem. Ber.* **1907**, *40*, 1145–1148.
- (3) Snider, B. B. Intramolecular Cycloaddition Reactions of Ketenes and Keteniminium Salts with Alkenes. *Chem. Rev.* **1988**, *88*, 793–811.
- (4) Tidwell, T. T. Ketene Chemistry: The Second Golden Age. *Acc. Chem. Res.* **1990**, *23*, 273–279.
- (5) Tidwell, T. T. Blue, But not a Mirage: Stable Aminoketenes by Carbene Carbonylation. *Angew. Chem., Int. Ed.* **2006**, *45*, 5580–5582.
- (6) Tidwell, T. T. Ketene Chemistry After 100 Years: Ready for a New Century. *Eur. J. Org. Chem.* **2006**, *2006*, 563–576.
- (7) Liang, Y.; Jiao, L.; Zhang, S. W.; Xu, J. X. Microwave- and Photoirradiation-Induced Staudinger Reactions of Cyclic Imines and Ketenes Generated from α -Diazoketones. A Further Investigation into the Stereochemical Process. *J. Org. Chem.* **2005**, *70*, 334–337.
- (8) France, S.; Weatherwax, A.; Taggi, A. E.; Lectka, T. Advances in the Catalytic, Asymmetric Synthesis of β -Lactams. *Acc. Chem. Res.* **2004**, *37*, 592–600.
- (9) Reddy, L. R.; Corey, E. J. Novel Bicyclization Reaction Leading to a Fused β -Lactone. *Org. Lett.* **2006**, *8*, 1717–1719.
- (10) McCaleb, K. L.; Halcomb, R. L. Intramolecular Ketene-Allene Cycloadditions. *Org. Lett.* **2000**, *2*, 2631–2634.
- (11) Tidwell, T. T. *Ketenes*; Wiley: New York, 1995.
- (12) Tidwell, T. T. *Ketenes II*; Wiley: New York, 2006.
- (13) Lee, S. Y.; Kulkarni, Y. S.; Burbaum, B. W.; Johnston, M. I.; Sinder, B. B. Type I Intramolecular Cycloadditions of Vinylketenes. *J. Org. Chem.* **1988**, *53*, 1848–1855.
- (14) Evans, D. A.; Janey, J. M. C-2-Symmetric Cu(II) Complexes as Chiral Lewis Acids. Catalytic, Enantioselective Cycloadditions of Silyl Ketenes. *Org. Lett.* **2001**, *3*, 2125–2128.
- (15) Zhao, C. X.; Mitchell, T. A.; Vallakati, R.; Perez, L. M.; Romo, D. Mechanistic Investigations of the ZnCl₂-Mediated Tandem Mukaiyama Aldol Lactonization: Evidence for Asynchronous, Concerted Transition States and Discovery of 2-Oxopyridyl Ketene Acetal Variants. *J. Am. Chem. Soc.* **2012**, *134*, 3084–3094.
- (16) Rasik, C. M.; Brown, M. K. Lewis Acid-Promoted ketene–alkene [2 + 2] Cycloadditions. *J. Am. Chem. Soc.* **2013**, *135*, 1673–1676.
- (17) Cheong, P. H. Y.; Legault, C. Y.; Um, J. M.; Celebi-Olcum, N.; Houk, K. N. Quantum Mechanical Investigations of Organocatalysis: Mechanisms, Reactivities, and Selectivities. *Chem. Rev.* **2011**, *111*, 5042–5137.
- (18) Douglas, J.; Taylor, J. E.; Churchill, G.; Slawin, A. M. Z.; Smith, A. D. NHC-Promoted Asymmetric β -Lactone Formation from Arylalkylketenes and Electron-Deficient Benzaldehydes or Pyridine-carboxaldehydes. *J. Org. Chem.* **2013**, *78*, 3925–3938.
- (19) Wang, Y. K.; Liang, Y.; Jiao, L.; Du, D. M.; Xu, J. X. Do Reaction Conditions Affect the Stereoselectivity in the Staudinger Reaction? *J. Org. Chem.* **2006**, *71*, 6983–6990.
- (20) Wei, D. H.; Wang, L. G.; Tang, M. S. A DFT Study on the Thermal Reaction Mechanisms of Fluorobutanesulfonyl Azide with Pyrazine under Solvent Free Condition. *Comput. Theor. Chem.* **2011**, *968*, 39–43.
- (21) Wang, X. N.; Zhang, Y. Y.; Ye, S. Enantioselective Synthesis of Spirocyclic Oxindole- β -Lactones via N-Heterocyclic Carbene-Catalyzed Cycloaddition of Ketenes and Isatins. *Adv. Synth. Catal.* **2010**, *352*, 1892–1895.
- (22) Wang, X. N.; Shao, P. L.; Lv, H.; Ye, S. Enantioselective Synthesis of β -Trifluoromethyl- β -Lactones via NHC-Catalyzed ketene–ketone Cycloaddition Reactions. *Org. Lett.* **2009**, *11*, 4029–4031.
- (23) Pons, J. M.; Pommier, A.; Rajzmann, M.; Liotard, D. Exploratory Theoretical-Study of the [2 + 2] Cycloaddition between Ketene and Formaldehyde. *J. Mol. Struct.: THEOCHEM* **1994**, *119*, 361–364.
- (24) Truong, T. N. Solvent Effects on Structure and Reaction Mechanism: A Theoretical Study of [2 + 2] Polar Cycloaddition between Ketene and Imine. *J. Phys. Chem. B* **1998**, *102*, 7877–7881.
- (25) Li, X. Y.; Xu, J. X. Annuloselectivity in Cycloadditions of Ketenes with Imines: A DFT Study. *J. Org. Chem.* **2013**, *78*, 347–355.
- (26) Wang, X. B.; Houk, K. N. Carbenoid Character in Transition Structures for Reactions of Ketenes with Alkenes. *J. Am. Chem. Soc.* **1990**, *112*, 1754–1756.
- (27) Kamiya, K.; Matsui, T.; Sugimura, T.; Shigeta, Y. Theoretical Insight into Stereoselective Reaction Mechanisms of 2,4-Pentanediol-Tethered Ketene-Olefin [2 + 2] Cycloaddition. *J. Phys. Chem. A* **2012**, *116*, 1168–1175.
- (28) Burke, L. A. Theoretical Study of [2 + 2] Cycloadditions. Kentene with Ethylene. *J. Org. Chem.* **1985**, *50*, 3149–3155.
- (29) Valenti, E.; Pericas, M. A.; Moyano, A. A Theoretical-Study on Ketene-Olefin Cycloadditions 0.1. Intermolecular Reactions. *J. Org. Chem.* **1990**, *55*, 3582–3593.
- (30) Cossio, F. P.; Ugalde, J. M.; Lopez, X.; Lecea, B.; Palomo, C. A Semiempirical Theoretical-Study on the Formation of β -Lactams from Ketenes and Imines. *J. Am. Chem. Soc.* **1993**, *115*, 995–1004.
- (31) Lecea, B.; Arrieta, A.; Arrastia, I.; Cossio, F. P. Origins of Stereocontrol in the [2 + 2] Cycloaddition between Achiral Ketenes and Chiral α -Alkoxy Aldehydes. A Pericyclic Alternative to the Aldol Reaction. *J. Org. Chem.* **1998**, *63*, 5216–5227.
- (32) Arrieta, A.; Lecea, B.; Cossio, F. P. Origins of the Stereodivergent Outcome in the Staudinger Reaction between Acyl Chlorides and Imines. *J. Org. Chem.* **1998**, *63*, 5869–5876.
- (33) Palomo, C.; Ganboa, I.; Kot, A.; Dembkowski, L. Practical Access to Carbacephem Intermediates via Asymmetric [2 + 2] Ketene-Imine Cycloaddition. *J. Org. Chem.* **1998**, *63*, 6398–6400.
- (34) Alajarín, M.; Vidal, A.; Tovar, F.; Arrieta, A.; Lecea, B.; Cossio, F. P. Surpassing Torquoelectronic Effects in Conrotatory Ring Closures: Origins of Stereocontrol in Intramolecular Ketenimine-Imine [2 + 2] Cycloadditions. *Chem.—Eur. J.* **1999**, *5*, 1106–1117.
- (35) Machiguchi, T.; Hasegawa, T.; Ishiwata, A.; Terashima, S.; Yamabe, S.; Minato, T. Ketene Recognizes 1,3-Dienes in their s-cis Forms through [4 + 2] (Diels-Alder) and [2 + 2] (Staudinger)

- Reactions. An Innovation of Ketene Chemistry. *J. Am. Chem. Soc.* **1999**, *121*, 4771–4786.
- (36) Arrieta, A.; Cossio, F. P.; Lecea, B. New Insights on the Origins of the Stereocontrol of the Staudinger Reaction: [2 + 2] Cycloaddition between Ketenes and N-silylimines. *J. Org. Chem.* **2000**, *65*, 8458–8464.
- (37) Venturini, A.; Gonzalez, J. A CASPT2 and CASSCF Approach to the Cycloaddition of Ketene and Imine: A New Mechanistic Scheme of the Staudinger Reaction. *J. Org. Chem.* **2002**, *67*, 9089–9092.
- (38) Machiguchi, T.; Okamoto, J.; Takachi, J.; Hasegawa, T.; Yamabe, S.; Minato, T. Exclusive Formation of α -Methylenoetanes in ketene–alkene Cycloadditions. Evidence for Intervention of both an α -Methylenoetane and the Subsequent 1,4-Zwitterion. *J. Am. Chem. Soc.* **2003**, *125*, 14446–14448.
- (39) Ramirez-Galicia, G.; Rubio, M. F.; Jimenez-Cruz, F. Intramolecular Competition between Alkenes in ketene–alkene [2 + 2] Cycloaddition. A Theoretical Study. *J. Mol. Struct.: THEOCHEM* **2006**, *773*, 53–58.
- (40) Cossio, F. P.; Arrieta, A.; Sierra, M. A. The Mechanism of the Ketene-Imine (Staudinger) Reaction in its Centennial: Still an Unsolved Problem? *Acc. Chem. Res.* **2008**, *41*, 925–936.
- (41) Lecea, B.; Arrieta, A.; Lopez, X.; Ugalde, J. M.; Cossio, F. P. On the Stereochemical Outcome of the Catalyzed and Uncatalyzed Cycloaddition Reaction between Activated Ketenes and Aldehydes to Form cis-2-Oxetanones and trans-2-Oxetanones - an Ab-Initio Study. *J. Am. Chem. Soc.* **1995**, *117*, 12314–12321.
- (42) Lecea, B.; Arrieta, A.; Roa, G.; Ugalde, J. M.; Cossio, F. P. Catalytic and Solvent Effects on the Cycloaddition Reaction between Ketenes and Carbonyl-Compounds to Form 2-Oxetanones. *J. Am. Chem. Soc.* **1994**, *116*, 9613–9619.
- (43) Pons, J. M.; Oblin, M.; Pommier, A.; Rajzmann, M.; Liotard, D. Formation of β -Lactones through Lewis Acid-Promoted [2 + 2] Cycloaddition Reaction. A Theoretical Study. *J. Am. Chem. Soc.* **1997**, *119*, 3333–3338.
- (44) Yamabe, S.; Minato, T.; Osamura, Y. Dual One-centre Frontier-orbital Interactions in [2 + 2] Cycloadditions of Ketenes. *J. Chem. Soc., Chem. Commun.* **1993**, *5*, 450–452.
- (45) Yamabe, S.; Kuwata, K.; Minato, T. Frontier-orbital Analyses of Ketene [2 + 2] Cycloadditions. *Theor. Chem. Acc.* **1999**, *102*, 139–146.
- (46) Wei, D. H.; Zhang, W. J.; Zhu, Y. Y.; Tang, M. S. A DFT Study on the Reaction Mechanisms of ketene–ketone [2 + 2 + 2] Cycloaddition to Form 3-Aryglutaric Anhydrides under A Lewis Acid Catalysis: What Is the Role of BF_3 ? *J. Mol. Catal. A: Chem.* **2010**, *326*, 41–47.
- (47) Asatryan, R.; Ruckenstein, E. Mechanism of Iron Carbonyl-catalyzed Hydrogenation of Ethylene. I. Theoretical Exploration of Molecular Pathways. *J. Phys. Chem. A* **2013**, *117*, 10912–10932.
- (48) Zhang, W. J.; Zhu, Y. Y.; Wei, D. H.; Tang, M. S. Mechanisms of the Cascade Synthesis of Substituted 4-amino-1,2,4-triazol-3-one from Huisgen Zwitterion and Aldehyde Hydrazone: A DFT Study. *J. Comput. Chem.* **2012**, *33*, 715–722.
- (49) Qiao, Y.; Han, K. L. Elucidation of the Reaction Mechanisms and Diastereoselectivities of Phosphine-Catalyzed [4 + 2] Annulations between Alenoates and Ketones or Aldimines. *Org. Biomol. Chem.* **2012**, *10*, 7689–7706.
- (50) Zhang, W. J.; Zhu, Y. Y.; Wei, D. H.; Li, Y. X.; Tang, M. S. Theoretical Investigations toward the [4 + 2] Cycloaddition of Ketenes with N-Benzoyldiazenes Catalyzed by N-Heterocyclic Carbenes: Mechanism and Enantioselectivity. *J. Org. Chem.* **2012**, *77*, 10729–10737.
- (51) Chen, H.; Wang, Z. F.; Zhang, Y. N.; Huang, Y. Highly trans-Stereoselective Synthesis of Bicyclic Isoxazolidines via Copper-Catalyzed Triple Cascade Catalysis. *J. Org. Chem.* **2013**, *78*, 3503–3509.
- (52) Paranjothy, M.; Siebert, M. R.; Hase, W.; Bachrach, S. M. Mechanism of Thiolate-Disulfide Exchange: Addition-Elimination or Effectively SN_2 ? Effect of a Shallow Intermediate in Gas-Phase Direct Dynamics Simulations. *J. Phys. Chem. A* **2012**, *116*, 11492–11499.
- (53) Bernstein, E. R.; Yu, Z. J. On the Decomposition Mechanisms of New Imidazole-Based Energetic Materials. *J. Phys. Chem. A* **2013**, *117*, 1756–1764.
- (54) Wei, D. H.; Lei, B. L.; Tang, M. S.; Zhan, C. G. Fundamental Reaction Pathway and Free Energy Profile for Inhibition of Proteasome by Epoxomicin. *J. Am. Chem. Soc.* **2012**, *134*, 10436–10450.
- (55) Wei, D. H.; Fang, L.; Tang, M. S.; Zhan, C. G. Fundamental Reaction Pathway for Peptide Metabolism by Proteasome. *J. Phys. Chem. B* **2013**, *117*, 13418–13434.
- (56) Wei, D. H.; Huang, X. Q.; Liu, J. J.; Tang, M. S.; Zhan, C. G. Reaction Pathway and Free Energy Profile for Papain-Catalyzed Hydrolysis of N-acetyl-Phe-Gly 4-Nitroanilide. *Biochemistry* **2013**, *52*, 5145–5154.
- (57) Zhang, W. J.; Truhlar, D. G.; Tang, M. S. Tests of Exchange-Correlation Functional Approximations Against Reliable Experimental Data for Average Bond Energies of 3d Transition Metal Compounds. *J. Chem. Theory Comput.* **2013**, *9*, 3965–3977.
- (58) Taylor, W. S.; Abrams, M. L.; Matthews, C. C.; Byers, S.; Musial, S.; Nichols, C. M. State-Specific Reactions of $\text{Cu}^+(\text{I}^{\text{S}}, \text{D})$ with CH_3X and CF_3X ($\text{X} = \text{Cl}, \text{Br}, \text{I}$): Exploring the Influence of Dipole Orientation on Association and C-X Bond Activation. *J. Phys. Chem. A* **2012**, *116*, 3979–3988.
- (59) Liu, Z.; Cheng, R. H.; He, X. L.; Wu, X. J.; Liu, B. P. DFT Functional Benchmarking on the Energy Splitting of Chromium Spin States and Mechanistic Study of Acetylene Cyclotrimerization over the Phillips Cr(II)/Silica Catalyst. *J. Phys. Chem. A* **2012**, *116*, 7538–7549.
- (60) Asatryan, R.; Bozzelli, J. W.; Ruckenstein, E. Dihydrogen Catalysis: A Degradation Mechanism for N_2 -Fixation Intermediates. *J. Phys. Chem. A* **2012**, *116*, 11618–11642.
- (61) Liu, S.; Srinivasan, S.; Grady, M. C.; Soroush, M.; Rappe, A. M. Computational Study of Cyclohexanone-Monomer Co-initiation Mechanism in Thermal Homo-polymerization of Methyl Acrylate and Methyl Methacrylate. *J. Phys. Chem. A* **2012**, *116*, 5337–5348.
- (62) Frisch, M. J.; Trucks, G. W.; Schlegel, H. B.; Scuseria, G. E.; Robb, M. A.; Cheeseman, J. R.; Scalmani, G.; Barone, V.; Mennucci, B.; Petersson, G. A. et al. *Gaussian 09*, revision C.01; Gaussian, Inc.: Wallingford, CT, 2010.
- (63) Becke, A. D. Density-Functional Thermochemistry 0.3. The Role of Exact Exchange. *J. Chem. Phys.* **1993**, *98*, 5648–5652.
- (64) Lee, C. T.; Yang, W. T.; Parr, R. G. Development of the Colle-salvetti Correlation-Energy Formula into a Functional of the Electron-Density. *Phys. Rev. B* **1988**, *37*, 785–789.
- (65) Miehlich, B.; Savin, A.; Stoll, H.; Preuss, H. Results Obtained with the Correlation-Energy Density Functionals of Becke and Lee, Yang and Parr. *Chem. Phys. Lett.* **1989**, *157*, 200–206.
- (66) Barone, V.; Cossi, M. Quantum Calculation of Molecular Energies and Energy Gradients in Solution by a Conductor Solvent Model. *J. Phys. Chem. A* **1998**, *102*, 1995–2001.
- (67) Mennucci, B.; Tomasi, J. Continuum Solvation Models: A New Approach to the Problem of Solute's Charge Distribution and Cavity Boundaries. *J. Chem. Phys.* **1997**, *106*, 5151–5158.
- (68) Gonzalez, C.; Schlegel, H. B. Reaction-Path Following in Mass-Weighted Internal Coordinates. *J. Phys. Chem.* **1990**, *94*, 5523–5527.
- (69) Gonzalez, C.; Schlegel, H. B. An Improved Algorithm for Reaction-Path Following. *J. Chem. Phys.* **1989**, *90*, 2154–2161.
- (70) Wei, D. H.; Zhu, Y. Y.; Zhang, C.; Sun, D. Z.; Zhang, W. J.; Tang, M. S. A DFT Study on Enantioselective Synthesis of Aza- β -Lactams via NHC-catalyzed [2 + 2] Cycloaddition of Ketenes with Diazenedicarboxylates. *J. Mol. Catal. A: Chem.* **2011**, *334*, 108–115.
- (71) Guo, L. First-Principles Study of Molecular Hydrogen Adsorption and Dissociation on Al_nCr ($n = 1–13$) Clusters. *J. Phys. Chem. A* **2013**, *117*, 3458–3466.
- (72) Vektarine, A. Insights into the Mechanism of the Benzoannelated Thieno[3,2-b]Furan Halogenation. Importance of HOMO-HOMO Interaction. *J. Phys. Chem. A* **2013**, *117*, 8449–8458.
- (73) Pfaendtner, J.; Fleming, K. L. Characterizing the Catalyzed Hydrolysis of β -1,4-Glycosidic Bonds Using Density Functional Theory. *J. Phys. Chem. A* **2013**, *117*, 14200–14208.

- (74) Yamabe, S.; Dai, T.; Minato, T.; Machiguchi, T.; Hasegawa, T. Ketene Is a Dienophile for [4 + 2] (Diels-Alder) Reaction across Its C=O Bond. *J. Am. Chem. Soc.* **1996**, *118*, 6518–6519.
- (75) Fang, D. C.; Fu, X. Y. Ab Initio Study on the Mechanism of Cycloaddition Reaction of Ketene with Methylenimine: A New Reaction Scheme. *Int. J. Quantum Chem.* **1992**, *43*, 669–676.
- (76) Parr, R. G.; Pearson, R. G. Absolute Hardness Companion Parameter to Absolute Electronegativity. *J. Am. Chem. Soc.* **1983**, *105*, 7512–7516.
- (77) Domingo, L. R.; Saez, J. A.; Zaragoza, R. J.; Arno, M. Understanding the Participation of Quadricyclane as Nucleophile in Polar [2 σ +2 σ +2 π] Cycloadditions toward Electrophilic π Molecules. *J. Org. Chem.* **2008**, *73*, 8791–8799.
- (78) Domingo, L. R.; Picher, M. T.; Saez, J. A. Toward an Understanding of the Unexpected Regioselective Hetero-Diels-Alder Reactions of Asymmetric Tetrazines with Electron-rich Ethylenes: A DFT Study. *J. Org. Chem.* **2009**, *74*, 2726–2735.
- (79) Domingo, L. R.; Aurell, M. J.; Perez, P.; Contreras, R. Quantitative Characterization of the Global Electrophilicity Power of Common Diene/Dienophile Pairs in Diels-Alder Reactions. *Tetrahedron* **2002**, *58*, 4417–4423.
- (80) Kohn, W.; Sham, L. J. Quantum Density Oscillations in an Inhomogeneous Electron Gas. *Phys. Rev.* **1965**, *137*, 1697–1705.
- (81) Sham, L. J.; Kohn, W. 1-Particle Properties of an Inhomogeneous Interacting Electron Gas. *Phys. Rev.* **1966**, *145*, 561–567.
- (82) Domingo, L. R.; Chamorro, E.; Perez, P. An Analysis of the Regioselectivity of 1,3-Dipolar Cycloaddition Reactions of Benzonitrile N-Oxides Based on Global and Local Electrophilicity and Nucleophilicity Indices. *Eur. J. Org. Chem.* **2009**, 3036–3044.
- (83) Domingo, L. R.; Chamorro, E.; Perez, P. An Understanding of the Electrophilic/Nucleophilic Behavior of Electro-Deficient 2,3-Disubstituted 1,3-Butadienes in Polar Diels-Alder Reactions. A Density Functional Theory Study. *J. Phys. Chem. A* **2008**, *112*, 4046–4053.
- (84) Domingo, L. R.; Perez, P.; Saez, J. A. Understanding the Local Reactivity in Polar Organic Reactions Through Electrophilic and Nucleophilic Parr Functions. *RSC Adv.* **2013**, *3*, 1486–1494.
- (85) Chamorro, E.; Perez, P.; Domingo, L. R. On the Nature of Parr Functions to Predict the Most Reactive Sites Along Organic Polar Reactions. *Chem. Phys. Lett.* **2013**, *582*, 141–143.